Astronomy & Astrophysics manuscript no. fdflae5˙7˙120406
April 12, 2006

Lyα emission galaxies at a redshift of z ≈ 5.7 in the FORS Deep Field ⋆

C. Tapken[1,3], I. Appenzeller[1], A. Gabasch[2,4], J. Heidt[1], U. Hopp[2,4], R. Bender[2,4], D. Mehlert[3], S. Noll[4], S. Seitz[2,4], and W. Seifert[1]

[1] Landessternwarte Heidelberg-Königstuhl, D-69117 Heidelberg, Germany
[2] Universitäts-Sternwarte München, Scheinerstr. 1, D-81679, München, Germany
[3] Max-Planck-Institut für Astronomie, Königstuhl 17, D-69117 Heidelberg, Germany
[4] Max-Planck-Institut für extraterrestrische Physik, Giessenbachstr., D-85741 Garching, Germany

received; accepted

ABSTRACT

Context. We present the results of a search for Lyα emission galaxies at z ≈ 5.7 in the FORS Deep Field.
Aims. The objective of this study is to improve the faint end of the luminosity function of high-redshift Lyα emitting galaxies and to derive properties of intrinsically faint Lyα emission galaxies in the young universe.
Methods. Using FORS2 at the ESO VLT and a set of special interference filters, we identified candidates for high-redshift Lyα galaxies. We then used FORS2 in spectroscopic mode to verify the identifications and to study their spectral properties.
Results. The narrow-band photometry resulted in the detection of 15 likely Lyα emission galaxies. Spectra with an adequate exposure time could be obtained for eight galaxies . In all these cases the presence of Lyα emission at $z = 5.7$ was confirmed spectroscopically. The line fluxes of the 15 candidates range between 3×10^{-21}Wm^{-2} and 16×10^{-21}Wm^{-2}, which corresponds to star-formation rates not corrected for dust between 1 and 5 M$_\odot$yr^{-1}. The luminosity function derived for our photometrically identified objects extends the published luminosity functions of intrinsically brighter Lyα galaxies.
Conclusions. With this technique the study of high-redshift Lyα emission galaxies can be extended to low intrinsic luminosities.

Key words. galaxies: high redshift – galaxies: emission lines

1. Introduction

The frequency and the physical parameters of high-redshift galaxies provide important constraints on the formation and evolution of these objects. Strong Lyα emission allows detection of Lyα emission galaxies (LAEs) at high redshift from their excess in narrow-band filters (e.g. Kudritzki et al. 2000; Rhoads et al. 2000; Steidel et al. 2000; Fynbo et al. 2003; Venemans et al. 2004). Apart from drop-out -selected galaxies (e.g., Lehnert & Bremer 2003; Bunker et al. 2004), our knowledge of the z > 5 galaxies is based on objects detected as emitters of strong Lyα radiation. Well-defined gaps in the telluric OH-bands allow to detect LAEs rather efficiently at very high redshifts (Hu et al. 1998; Taniguchi et al. 2003b; Maier et al. 2003; Ajiki et al. 2003; Rhoads et al. 2003; Taniguchi et al. 2005, Wang et al. 2005; for a review see Taniguchi et al. 2003a). These gaps appear around λ = 7110, 8160, 9210 Å corresponding to z≈ 4.8, z≈ 5.7 and z≈ 6.6 for LAEs. Particularly successful have been observations with the SuprimeCam of the Subaru telescope, leading, e.g., to the discovery of a large-scale structure at z≈5.7 (Ouchi et al. 2005). The properties of the LAEs have also been used to derive the luminosity function of LAEs (Hu et al. 2004), the star-formation rate in the early universe (Ajiki et al. 2003), and the epoch of re-ionization (Rhoads et al. 2004). However, so far, most detections of high-redshift LAEs have been based on relatively large area surveys sampling the intrinsically luminous objects. Only a few studies have been devoted to faint LAEs at high redshift. Santos et al. (2004) observed selected regions near intermediate-redshift clusters, finding eleven lensed low-luminosity LAEs between z = 2.2 and 5.6. Using a multi-slit technique, Martin et al. (2005) find ≈ 20 faint LAEs at z ≈ 5.7.

Although bright Lyα galaxies are relatively easy to detect, their nature and physical structure is not understood well. Since Lyα is a resonance line of the most abundant element, the mean free path of Lyα photons in the interstellar matter is short and the photons diffuse in physical and frequency space (Neufeld 1990). Hence, there is no straightforward correspondence between the properties of the Lyα emission and the physical properties of the emitting galaxy. Moreover, dust affects the Lyα

Send offprint requests to: C. Tapken, Heidelberg (e-mail: tapken@mpia.de)

⋆ Based on observations (Prop. ID: 071.A-0174(A) and 074.A-0237(A)) obtained at the ESO VLT at Cerro Paranal, Chile.

photons more strongly than the UV-continuum photons, which are not subject to resonance scattering (Charlot & Fall 1993). As dust absorption depends on the presence of heavy elements, one may expect to also find among the LAEs metal-poor or primordial matter galaxies with a stellar population different from local objects (Malhotra &Rhoads 2002). Because of the complex physics of the high-redshift Lyα emission galaxies, their relationship with the better-studied continuum-selected high-redshift galaxies (LBGs) (see, e.g., Shapley et al. 2003) is not understood well (Ouchi et al. 2004). A detailed derivation and comparison of the luminosity functions of LAEs and LBGs could help to clarify this relation. Furthermore, there are theoretical predictions that photoionization heats and removes gas from the gravitational wells of galaxies during the re-ionization period. This may suppressed the galaxy formation in low-mass halos (Barkana & Loeb 1999). A break in the luminosity function might be a tool for deriving the halo mass where the star-formation is suppressed (Santos et al. 2004) and other parameters of the re-ionization epoch.

We, therefore, carried out a search for intrinsically faint LAEs in the FORS Deep Field (FDF; Appenzeller et al. 2000; Heidt et al. 2003; Noll et al. 2004). Since the FDF covers an area of 7 ' × 7', only a few of the bright Lyα galaxies detected in most of the surveys quoted above can be expected to be found in the FDF. However, by extrapolating the known part of the LF (Hu et al. 2004), we expected (and verify with this paper) that a significant number of intrinsically faint Lyα emission galaxies are present in the FDF. A great advantage of the FDF with respect to other surveys is the availability of very deep broadband photometry and accurate photometric redshifts. The B, R, and I broad-band images have a limiting Vega magnitude (3σ in 2" diameter aperture) of 28.59, 27.99, and 27.21. These data allow a reliable discrimination between Lyα galaxies and other emission line objects.

Throughout this paper we use Vega magnitudes and adopt $\Omega_\Lambda = 0.7$, $\Omega_M = 0.3$, and $H_0 = 70$ km s^{-1}Mpc^{-1}. The probed redshift of $5.630 < z < 5.803$ results in a comoving volume of 1.5×10^4 Mpc^3.

2. Photometric data

2.1. Observations and data reduction

LAEs are identified by their redshifted Lyα emission with narrow-band imaging. The choice of the band-width of the narrow-band filter is a tradeoff between the sensitivity and the search volume (Maier et al. 2003). Three narrow-band filters placed in one atmospheric gap are a reasonable choice in terms of sensitivity and search volume. Furthermore they have the advantage of determining the continuum of the object near the emission line (Klaus Meisenheimer, priv. comm.). For the present study we acquired three interference filters with bandwidths of about 60 Å and central wavelengths of 8100 Å, 8150 Å, and 8230 Å with high effective transmissions (≈ 93 %) for the FORS2 multimode instrument at the ESO VLT. The three slightly overlapping filters fully cover the 8150 Å window of the telluric OH emission. Any object with emission lines in the wavelength range covered by the filters is expected to show an excess emission in one or (in cases where the emission coincides with an overlap wavelength) two of the filter bands. After completion of the present program, the filters are now publicly available. Their ESO designations are FILT_810_7+107, FILT_815_5+108, and FILT_823_6+109. In the following these designations will be abbreviated to F810, F815, and F823, respectively.

Table 1. Overview of the narrow-band observations. The ESO filter ID, their central wavelengths λ_c, their bandwidth *bw* (FWHM), the total integration time and the 50 % completeness limit are given.

Filter	λ_c [Å]	bw [Å]	Exp. time [s]	50 % compl. [mag]
FILT_810_7+107	8100	69	19800	25.56
FILT_815_5+108	8150	53	21240	25.63
FILT_823_6+109	8230	55	21240	25.67

All photometric observations were carried out in August 2003 in visitor mode with FORS2 at the VLT-Yepun. The detector was a mosaic of two 2k × 4k MIT CCDs used in the 200kHz readout mode with low gain and 2×2 binning. Each frame was integrated for 1800 s. The total integration times and other information are listed in Table 1. The seeing varied between 0.″5 and 0.″8.

The data were reduced using the codes and procedures described by Heidt et al. (2003). All images were smoothed to a common seeing of FWHM=0.″78 and co-added signal-to-noise weighted. The photometric calibration was done using standard stars with known spectra. The source detection was carried out on the co-added images using SExtractor (Bertin & Arnouts 1996), with the same parameters as for the I-band images (for details see Heidt et al. 2003). The number of significantly detected objects was 4303 in F810, 4519 in F815, and 4675 in F823. SExtractor was also used to derive total fluxes and magnitudes of the detected objects. 50% completeness limits for point sources were calculated following Snigula et al. (2002), using basic image and detection parameters. The completeness limits are listed in Table 1.

The three filter bands avoid the stronger OH emission features still present in the 8150 Å OH window by having most of these lines coincide with the low-sensitivity wings of the narrow bands. Therefore, the background is low, and lower emission-line-flux levels can be reached than is possible with a single narrow-band filter covering the 8150 Å OH window. Other factors contributing to the high sensitivity of the present survey are the small filter band widths, the high sensitivity of the FORS2 CCD at 8150 Å, and a better-than-average seeing during the observations. Moreover, all narrow-band observations were made during the second half of the observing nights, when (due to the nocturnal decay) the OH airglow is on average weaker.

2.2. Selection of the LAE candidates

In order to find LAE candidates among the objects that were detected in the narrow band images we extracted in a first step all objects showing a statistically significant flux excess (relative

to the other bands) in one or two of the three narrow band images. Objects that had been detected in several filter bands were regarded as having a significant flux excess if a flux difference larger than 3 σ was found. As a next step we used the deep broad-band images, the FDF photometric catalog (Heidt et al. 2003), and the FDF photometric redshift catalog (Gabasch et al. 2004) to eliminate objects with $z < 5.7$ where emission lines other than Lyα coincided with our filter bands. In this way the great majority of the narrow-band excess objects could be identified as foreground objects on the basis of their reliably lower photometric (and in some cases spectroscopic) redshifts, blue flux, or too low an (R-I). The majority (85%) of the narrow-band excess objects showed a small narrow-band magnitude difference of < 1.2 mag. A significant fraction of these objects have narrow-band excess caused by continuum features (e.g. we found that cool stars can produce an excess flux in our narrow bands). Thus an excess flux in a narrow-band frame of 1.2 mag is required to select galaxies with a strong emission line. To select faint LAEs, we used for the final catalog of LAEs candidates the deep I-band image as a reference. About 50% of the excess objects with a narrow-band magnitude difference of > 1.2 mag could be identified as [OII] emitters at $z = 1.2$. Other narrow-band flux excess objects could be explained by [O III] or Balmer line emission. Among the narrow-band excess objects that could not be eliminated as LAE candidates was only one object listed in the Heidt et al. (2003) FDF photometric catalog. This object (FDF-2178, $z_{phot} = 5.74$) shows a marginally significant flux excess in the F823 filter and an R-I > 2.2. However, its flux in the F815 and F810 bands is too high to be consistent with the expected drop shortward of Lyα. Hence we conclude that this object, although certainly a high redshift galaxy, is not a $z = 5.7$ LAE candidate.

The final catalog of LAEs candidates was selected in the following way. First we selected all objects showing a 3 σ flux excess (relative to the other bands) in one or two of the three narrow-band images. The narrow-band excess objects have to satisfy the following criteria to be regarded as LAEs candidates: (1): NB < 25.7 mag, (2): I-NB > 1.2 mag, (3): no detection in the B band. Bright objects (I < 25.5 mag) had to fulfill the criterion (4a): R-I > 1.5 mag and faint objects the criterion (4b): no detection in the R band. Fiffteen narrow-band excess objects meet the criteria (1)-(4) and are listed in Table 2. In the following the individual objects are referred to by their sequence number in this table. The magnitudes given in Table 2 are narrow-band magnitudes in the Vega system. Also included in Table 2 are Lyα equivalent widths (EW) derived (as described in Sect. 4.3) from the photometric data and photometric and (where available) spectroscopic Lyα line fluxes. The spectroscopic fluxes do not include corrections due to possible slit losses. Some of the objects in the table are visible on the FDF I-band and z-band images (however, in none of the bluer band images) but have I-band fluxes below the 5 σ limit. Therefore, none of objects in Table 2 is listed in the Heidt et al. (2003) FDF photometric catalog.

From a visual control of other crowded regions of the narrow-band images, we regard it as unlikely that many LAE candidates have been missed by this selection criteria. Examples of the B, I, F810, F815, and F823 images are presented in Fig. 1. An atlas of all objects in Table 2 in these filters is given in Fig. 9 (available in electronic form only).

3. Spectroscopic data

3.1. Observations and reduction

Originally we planned to carry out a spectroscopic verification of all LAE candidates in Table 2 using FORS2 in spectroscopic mode. Because of the high red efficiency of the FORS2 detector and the FORS2 VPH gratings, a spectroscopic detection of the Lyα flux (as estimated from the narrow-band data) of all our LAE candidates can be achieved with a modest amount of observing time with this instrumentation. An adequate amount of service observing time was granted for this program by the ESO OPC in 2004. However, due to the pressure of higher priority programs only a small fraction of our priority B program could actually be executed in November 2004. An application for additional time to complete the program was not successful.

For the spectroscopic observations obtained in November 2004, we used the holographic grism 1028z, covering the wavelength range 7800 - 9300 Å at a resolution (with a 1" slit width) of R ≈ 2700 ($\Delta v \approx 110$ kms^{-1}). This resolution allows a good subtraction of weak OH lines and a reliable identification of foreground [O II] emission objects (see Fig. 2i). To observe all 15 objects with an adequate S/N, three different MOS masks had been prepared, with the intention of exposing each mask for three hours. By including the fainter objects in all three masks, while the brighter targets were included in only one mask, it was planned to detect all targets with an adequate SNR. For the reasons described above, only one mask could be exposed with total integration time of 2.7 h only.

The spectra were reduced using MIDAS and the routines developed by Noll et al. (2004). The two-dimensional spectra were corrected with a dome flatfield and were wavelength-calibrated using the calibration spectra of gas discharge lamps. After the extraction of the one-dimensional spectra, a flux calibration was carried out using spectra of standard stars observed during the same night. The one-dimensional spectra were then co-added. Since the efficiency of VPH grisms varies with the angle of incidence and thus with the object's position in the telescope focal plane (see Tapken 2005), the fluxes were corrected for this using the sky-background. For 8000 - 8200 Å, this effect was below 10 % for most spectra.

3.2. Spectroscopic results

The single MOS mask for which data could be obtained included eight of the LAE candidates of Table 2 and several calibration and reference objects. In spite of the short exposure time, line emission from all of these eight LAE candidates was detected. In each case only one single emission line was observed. Figure 2 shows the observed line profiles. Since all objects in Table 2 show only weak or no detectable continua, which could provide independent information on the redshift, we verified that our spectra do not contain additional emission lines that were expected in the case that the observed features were due to redshifted [O III] or Balmer lines. Moreover, none

Table 2. Photometric and spectroscopic properties of the 15 LAE candidates. The limits of the narrow-band photometry correspond to the limiting magnitude (3σ in 2" diameter aperture).

Nr.	RA	DEC	mag_{810}	mag_{815}	mag_{823}	$Flux_{phot}$ [10^{-21} Wm^{-2}]	EW [Å]	z_{spec}	$Flux_{spec}$ [10^{-21} Wm^{-2}]
1	1:05:50.36	-25:46:31.30	> 26.35	> 26.46	25.03 ± 0.11	5.41 ± 0.55	> 70.1	5.780	8.36 ± 0.83
2	1:05:51.06	-25:43:21.50	25.28 ± 0.16	24.75 ± 0.09	> 26.48	5.02 ± 0.37	> 99.5	-	-
3	1:05:52.24	-25:47:10.24	> 26.35	> 26.46	25.12 ± 0.14	4.98 ± 0.64	> 61.8	5.770	2.41± 0.49
4	1:05:52.45	-25:43:52.50	> 26.35	> 26.46	24.61 ± 0.10	7.97 ± 0.73	> 131.5	-	-
5	1:05:53.42	-25:44:26.42	> 26.35	> 26.46	24.88 ± 0.10	6.22 ± 0.57	> 86.9	-	-
6	1:05:54.94	-25:48:25.08	> 26.35	> 26.46	25.14 ± 0.15	4.89 ± 0.68	> 60.1	5.787	8.17 ± 1.02
7	1:05:58.45	-25:42:41.17	24.73 ± 0.10	> 26.46	> 26.48	9.02 ± 0.83	> 161.4	-	-
8	1:05:59.27	-25:49:20.37	24.82 ± 0.11	> 26.46	> 26.48	8.30 ± 0.84	> 138.0	5.627	4.79± 0.56
9	1:06:01.46	-25:44:25.45	25.16 ± 0.13	> 26.46	> 26.48	6.07 ± 0.73	> 80.7	-	-
10	1:06:06.05	-25:43:17.68	> 26.35	> 26.46	25.69 ± 0.19	2.95 ± 0.52	> 28.4	-	-
11	1:06:07.82	-25:48:49.86	> 26.35	> 26.46	25.07 ± 0.13	5.22 ± 0.62	> 66.3	5.758	1.13 ± 0.33
12	1:06:07.93	-25:43:17.47	> 26.35	24.26 ± 0.05	> 26.48	10.59 ± 0.49	> 230.1	-	-
13	1:06:08.88	-25:48:37.24	> 26.35	24.83 ± 0.11	> 26.48	6.26 ± 0.63	>88.4	5.679	4.37 ± 0.50
14	1:06:09.38	-25:48:20.32	> 26.35	> 26.46	25.00 ± 0.15	5.57 ± 0.77	> 73.1	5.764	4.05 ± 0.54
15	1:06:16.29	-25:48:06.58	24.1 ± 0.05	> 26.46	> 26.48	16.12 ± 0.74	> 872.4	5.640	11.99 ± 0.72

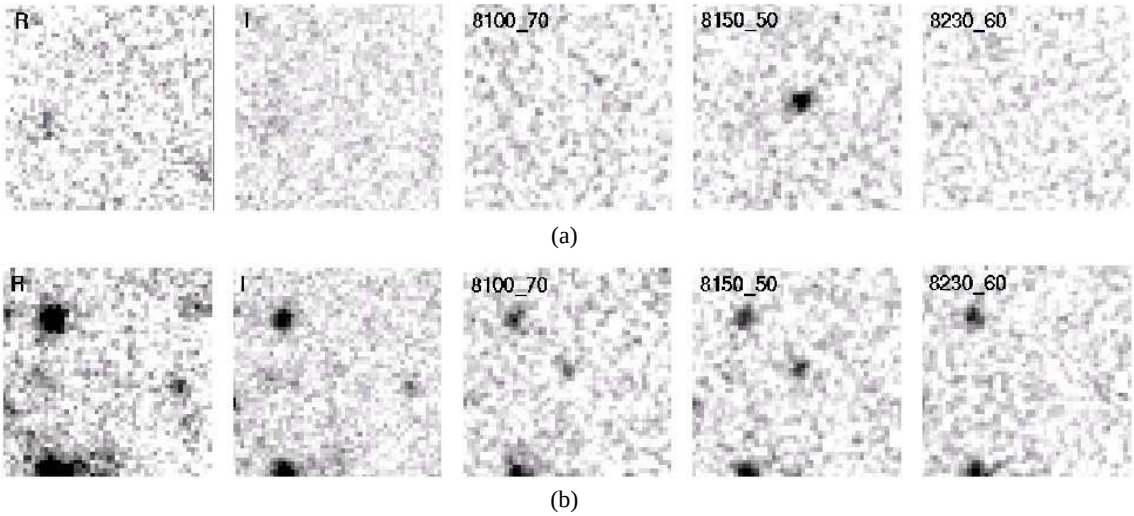

Fig. 1. Bessel-R, Bessel-I broad-band images and F810, F815, and F823 narrow-band images of 2 examples of our targets: (a) The second brightest candidate (No. 12) . (b) Object with an intermediate flux and visible in two narrow-band filters, although it was significantly detected only in the F815 filter (No. 13). Each image shows a 10" × 10" area centered on the target.

of the profiles has the structure expected for the [O II] 3727 Å doublet. This doublet has a rest-frame separation of 2.8 Å, leading to an observed doublet separation of ≈ 6 Å, allowing for an easy separation at our resolution. As an example at the end of Fig. 2 we include the [O II] doublet of FDF-7757 (z_{phot} = 1.22) observed during the same run. Only our LAE candidate No. 13 shows an apparent (but not significant) doublet structure of the expected width. However if this line was indeed [O II], the doublet ratio would hardly be consistent with the theoretically allowed range of values (Osterbrock 1989).

4. Properties of the LAE candidates

4.1. Spatial and redshift distribution

Figure 3 shows the spatial distribution of our LAE candidates. The objects are clustered at the edge of the field, while the center seems to be avoided. We verified that this distribution is not caused by reduction problems by comparing the limiting magnitudes in the de-voided area with the limiting magnitude in the area containing the objects. Our sample is too small to verify that this distribution deviates significantly from a random distribution. However, our result is consistent with the data of Hu et al. (2004) covering of a ≈ 10 times larger volume, who find evidence for large-scale structure of the bright LAEs distribution and Wang et al. (2005), who find an overdensity of LAEs in the Chandra Deep Field South.

The distribution of spectroscopic redshifts within the observational window is given in Fig. 4. A high fraction of F823 candidates were included in the mask observed, thus most of the redshifts in Fig. 4 are clustered at z ≈ 5.76.

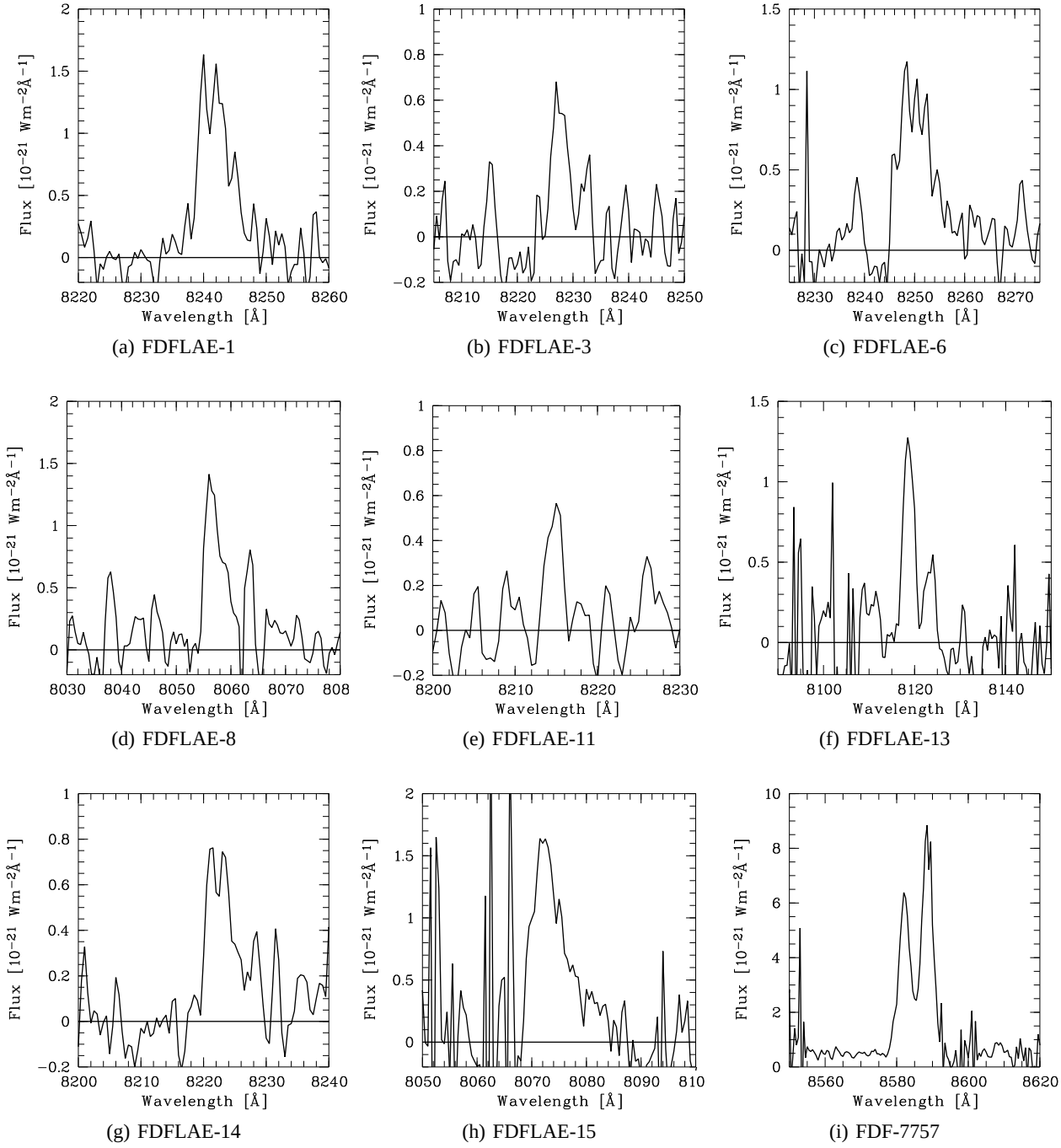

(a) FDFLAE-1 (b) FDFLAE-3 (c) FDFLAE-6

(d) FDFLAE-8 (e) FDFLAE-11 (f) FDFLAE-13

(g) FDFLAE-14 (h) FDFLAE-15 (i) FDF-7757

Fig. 2. Observed emission line profiles of the LAE candidates. For comparison the [OII] 3727 doublet of FDF-7757 at z_{phot} = 1.22 is also included.

4.2. Fluxes and star-formation rates

The line fluxes are derived using the narrow-band photometry. In Fig. 5 the distribution of fluxes is shown. The fluxes range from 3×10^{-21}Wm^{-2} to 16×10^{-21}Wm^{-2}. All fluxes are below the flux limit of Hu et al. (2004) of 20×10^{-21}Wm^{-2}.

From the flux of the Lyα line we computed star-formation rates. The line luminosities are derived by assuming a cosmology model ($\Omega_\Lambda = 0.7$, $\Omega_M = 0.3$, and $H_0 = 70$ km s^{-1}Mpc^{-1}) and isotropic emission. To derive the star-formation rates, the calibration of Kennicutt (1998)[1] was used and Case B recombination was assumed. In Fig. 6 the distribution of the star-formation rates is given. The star-formation rates derived from the line fluxes are between 1 and 5 M$_\odot$yr^{-1}. As pointed out above, part of the Lyα may be lost by dust absorption. Moreover, the intergalactic medium probably absorbs a fraction of the Lyα photons. Hence the observed line luminosity

[1] Kennicutt (1998) assumes a Salpeter initial mass function in the mass range of 0.1 to 100 M$_\odot$, solar metalicity, and a 100 Myr old starburst with continuous star-formation.

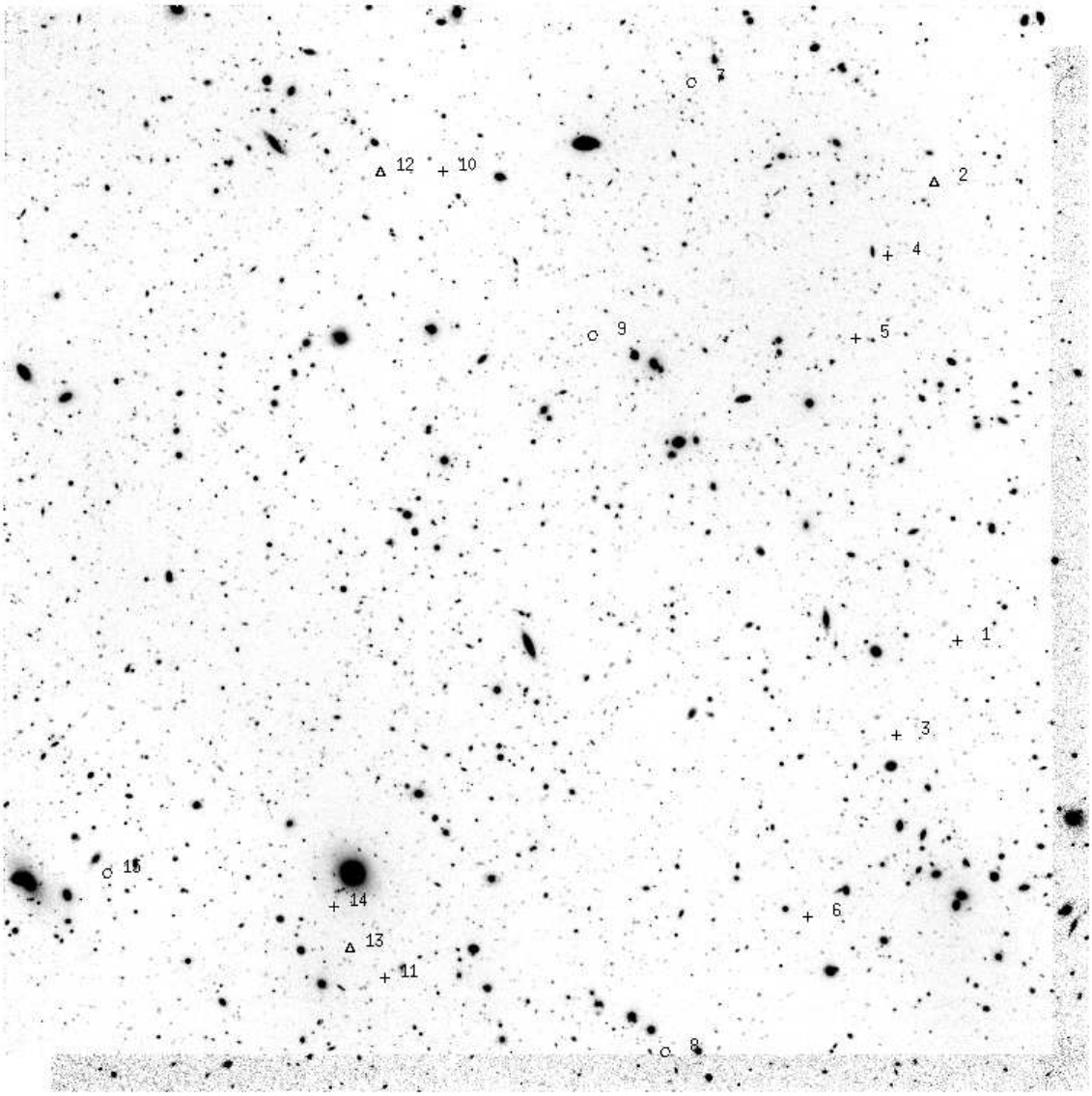

Fig. 3. The spatial distribution of the narrow-line excess objects in the FDF (shown is a deep I-band image). Circles correspond to objects found in the narrow-band nb810, triangles to objects detected in the narrow-band nb815, and crosses to objects found in the narrow-band nb823. North is up, east is left. The field is 7 × 7 arcminutes large, which corresponds to 2.5 Mpc × 2.5 Mpc (physical) or 17 Mpc × 17 Mpc (comoving).

and thus the star-formation rates are only lower limits. In addition, the conversion of line luminosity into star-formation rates depends on assumptions of the starburst properties and the IMF.

4.3. Equivalent widths

Using the I-band and the narrow-band photometric results, we tried to calculate Lyα equivalent widths or lower limits for all our LAE candidates. For this task we used the procedure described by Hu et al. (2004). This approach based on the assumption of a rectangular filter shape of the I-band and the assumption that the I-band flux represents the continuum. The latter may be a poor approximation in our case. We re-measured the I-band magnitudes for all LAE candidates using aperture photometry. Although several objects are visible on the I-band image, only four were marginally detected with $2 < \sigma < 3$. For all objects, the three sigma detection limit in a 2" diameter aperture was used as an upper limit for the continuum. In Table 2 we list the resulting rest-frame equivalent widths and lower limits. As shown by the table, all objects have rest-frame equivalent widths >20 Å.

4.4. Line profiles

All observed line widths of our LAEs are below 300 kms^{-1}. This agrees with other spectroscopic studies of high-redshift LAEs (Dawson et al. 2004). High-redshift LAEs have also be identified in the literature on the basis of asymmetric line profiles, typically showing a sharp drop in the blue wing and an extended red wing (Dawson et al. 2002). Kunth et al. also

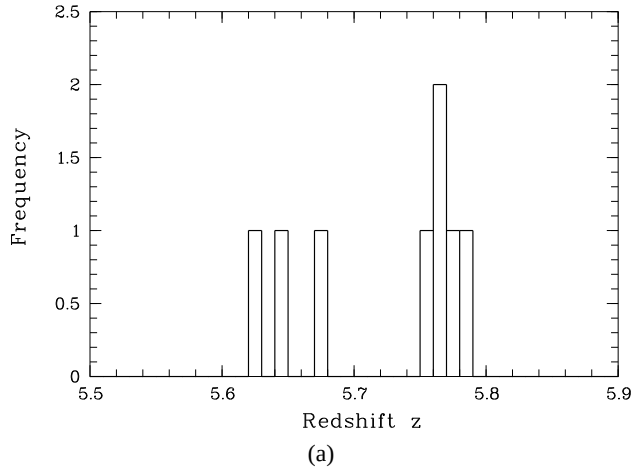

Fig. 4. Distribution of redshifts of the eight LAE candidates observed spectroscopically.

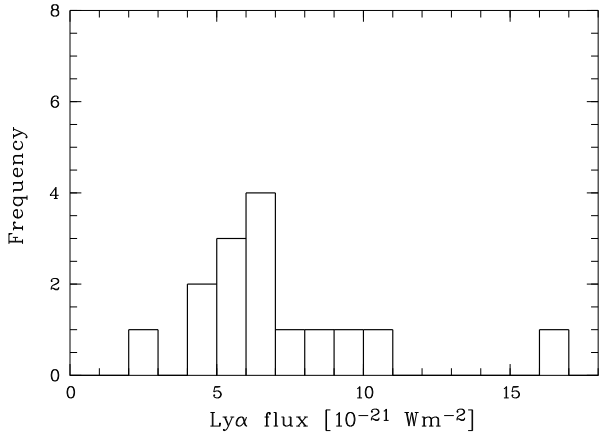

Fig. 5. The distribution of the photometric line fluxes of the 15 LAE candidates.

(1998) observed asymmetric Lyα profiles also in nearby star-forming galaxies. Hu et al. (2004) modeled the composite profile of 19 LAEs with a Gauss emission profile and a Voigt absorption. They attributed the absorption to the intergalactic medium. Most line profiles in Fig. 2 also show an asymmetry.

To quantify the asymmetry we used the parameters introduced by Rhoads et al. (2003) $a_{\rm flux}$ and $a_{\rm wave}$. $a_{\rm wave}$ gives the wavelength ratio and $a_{\rm flux}$ the flux ratio of the blue and red part of the Lyα profile:

$$a_{\rm flux} = \frac{\int_{\lambda_{10,\rm b}}^{\lambda_{\rm peak}} f(\lambda) d\lambda}{\int_{\lambda_{\rm peak}}^{\lambda_{10,\rm r}} f(\lambda) d\lambda} \quad (1)$$

and

$$a_{\rm wave} = \frac{(\lambda_{10,\rm r} - \lambda_{\rm peak})}{(\lambda_{\rm peak} - \lambda_{10,\rm b})}. \quad (2)$$

Here, $\lambda_{\rm peak}$ is defined as the wavelength of the peak of the emission. $\lambda_{10,\rm b}$ ($\lambda_{10,\rm r}$) is defined as the wavelength where the flux reaches 10 % of his peak flux level on the blue (red) side.

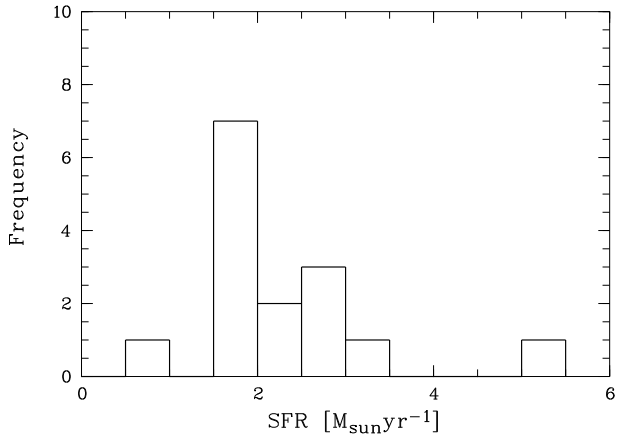

Fig. 6. The distribution of the star-formation rates derived from the photometric line fluxes.

For six lines we could measure the values of $a_{\rm flux}$ and $a_{\rm wave}$. Except for FDFLAE-13, all objects show that $a_{\rm flux}$ and $a_{\rm wave}$ are greater than 1, i.e., are extended to the red in good agreement with the results of Dawson et al. (2004), who mainly analysed galaxies with $z > 4$. Moreover, Dawson et al. (2004) found for 28 galaxies at $z \approx 1$ asymmetry parameters of the [OII] $\lambda\lambda$3726.2, 3728.9 line of $a_{\rm wave}$ and $a_{\rm flux} \approx 1$. In our sample FDFLAE-15 has the strongest asymmetry with $a_{\rm flux} = 3.91 \pm 0.57$ and $a_{\rm wave} = 1.64 \pm 0.26$. A composite spectrum formed by simply adding all our individual profiles is shown in Fig. 7. Obviously this composite also shows a marked asymmetry in the expected sense.

From the discussion above, we conclude that at least our LAE candidates with a spectroscopic confirmation are indeed LAEs at $z = 5.7$. The high success rate of our spectroscopic verifications suggests that at least the great majority of our all LAE candidates are LAEs at $z \approx 5.7$.

4.5. The luminosity function

Using the observed density of our LAE candidates in the FDF and assuming (for the reasons given above) that all these objects are LAEs, we can use the data of Table 2 to derive the surface and space density of the low-luminosity LAEs as a function of the luminosity (i.e. the LF). In order to avoid uncertain incompleteness corrections, we used for this purpose only those objects in Table 2 that have narrow-band magnitudes brighter than the 50 % completeness limit (14 of the 15 LAEs). The results are given in Fig. 8, together with the published luminosity function of Hu et al. (2004) and Ajiki et al. (2003) . Hu et al. (2004) used deep narrow-band imaging of the SSA22 field to search for 19 LAEs at a redshift of z=5.7. They detected 26 candidates down to a limited flux of 20×10^{-21}Wm^{-2}. Spectroscopic observations showed a high succes rate. Ajiki et al. (2003) found 20 LAE candidates at a redshift of z=5.7 with the Suprime-Cam. As shown by the figure, our luminosity function is consistent with a continuation of the Hu et al. and Ajiki et al. luminosity function towards lower luminosities. Malhotra & Rhoads (2004) assembled data from sev-

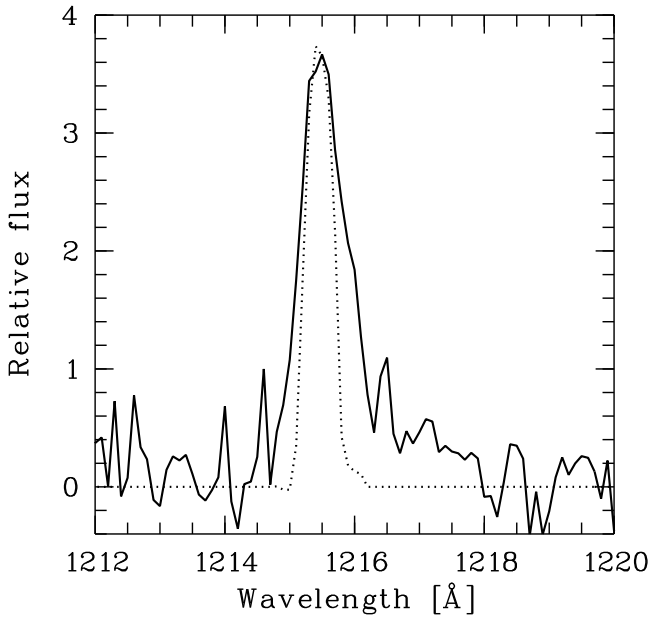

Fig. 7. Composite spectra of the eight emission line objects. The dotted line is the instrumental profile, derived from the sky lines.

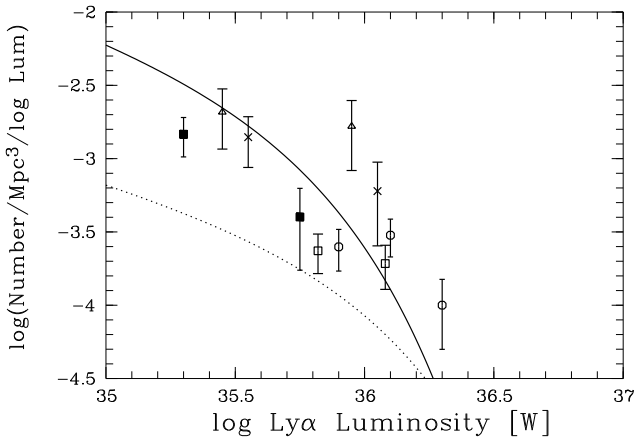

Fig. 8. Luminosity function derived from the photometric data (filled squares). Two surveys at a redshift of z = 5.7 have been included: Circles correspond to Hu et al. (2004) and open squares to Ajiki et al. (2003). Two surveys at a redshift of z≈ 3.2 are also included: triangles correspond to Kudritzki et al. (2000), crosses to Cowie & Hu (1998). Moreover a Schechter function (Breukelen et al. 2005) for Lyα emitters with $2.3 < z < 4.6$ (solid line) and a Schechter function (Malhotra & Rhoads 2004) for LAEs at z≈ 5.7 (dotted line) is plotted. The error bars denote statistical mean errors.

eral narrow-band LAEs surveys at a redshift of z ≈ 5.7 and derived a Schechter function (α = - 1.5, $L_\star = 10^{36}$ W, $\Phi_\star = 10^{-4}$ Mpc^{-3}) included in Fig. 8. We find more LAE candidates than expected on the basis of this luminosity function.

We also included in Fig. 8 the luminosity function from Kudritzki et al. (2000) and Cowie & Hu (1998). Kudritzki et al. (2000) and Cowie & Hu (1998) used the narrow-band technique to detect LAEs at a redshift of z=3.1 (3.4). Their results are largely consistent with the higher redshift luminosity function. Moreover, we included the Schechter function for Lyα emitters with $2.3 < z < 4.6$ (mean z = 3.18) derived by van Breukelen et al. (2005). Van Breukelen et al. (2005) detected 14 LAEs using VIMOS IFU spectroscopy. Their Schechter function is consistent with our results.

We also compared our number counts with the prediction of Thommes & Meisenheimer (2005), who compute the expected surface density of Lyα emitting galaxies on the assumption that LAEs are the progenitors of today's elliptical galaxies and bulges of spiral galaxies. One of the main assumptions of this model is a short Lyα bright phase of the star-forming galaxies. This short duration of the Lyα bright phase is explained by the rapid formation of dust in this galaxies. The basic model of Thommes & Meisenheimer (2005) predicts a number of ≈ 20 LAEs with $L_{\mathrm{Ly}\alpha} \geq 10^{35}$ W in the FORS Deep Field at a redshift of z≈ 5.7. Given the large uncertainity, this agrees with the observed number of 15.

5. Conclusions

Our survey has shown that FORS2, the ESO VLT, and our special filter set make it possible to extend groundbased searches for Lyα emission galaxies at z = 5.7 to significantly lower luminosities. Although the lack of observing time did not allow a full spectroscopic verification of all objects detected by our narrow-band filter survey, the available spectroscopic results indicate a high success rate of this set-up. The observed faint LAEs show very similar properties to those observed at higher luminosities. A luminosity function constructed on the assumption that all our photometrically detected emission objects are LAEs at z = 5.7 is in good agreement with the LF published by Hu et al. (2004) and extends the Hu et al. luminosity function towards lower luminosities.

Acknowledgements. We would like to thank the staff of the Paranal Observatory for carrying out the spectroscopic service observations. This research has been supported by the German Science Foundation DFG (SFB 439). We thank the referee for valuable comments.

References

Ajiki, M., Taniguchi, Y., Fujita, S. S., et al. 2003, AJ, 126, 2091
—. 2004, PASJ, 56, 597
Appenzeller, I., Bender, R., Böhm, A., et al. 2000, The Messenger, 100, 44
Barkana, R.,& Loeb, A. 1999, ApJ, 523, 54
Bertin, E., & Arnouts, S. 1996, A&AS, 117, 393
Bunker, A. J., Stanway, E. R., Ellis, R. S.,& McMahon, R. G. 2004, MNRAS, 355, 374
Charlot, S., & Fall, S. M. 1993, ApJ, 415, 580
Cowie, L. L., & Hu, E. M. 1998, AJ, 115, 1319
Dawson, S., Spinrad, H., Stern, D., et al. 2002, ApJ, 570, 92
Dawson, S., Rhoads, J. E., Malhotra, S., et al. 2004, ApJ, 617, 707
Fynbo, J. P. U., Ledoux, C., Möller, P., Thomsen, B., & Burud, I. 2003, A&A, 407, 147
Gabasch, A., Bender, R., Seitz, S., et al. 2004, A&A, 421, 41
Heidt, J., Appenzeller, I., Gabasch, A., et al. 2003, A&A, 398, 49
Hu, E. M., Cowie, L. L., McMahon, R. G. 1998, ApJL, 502, L99
Hu, E. M., Cowie, L. L., Capak, P., et al. 2004, AJ, 127, 563

Kennicutt, R. C., Jr. 1998, ARA&A, 36, 189
Kudritzki, R.-P., Méndez, R. H., Feldmeier, J. J., et al. 2000, ApJ, 536, 19
Kunth, D., Mas-Hesse, J. M., Terlevich, E., et al. 1998, A&A, 334, 11
Lehnert, M. D., & Bremer, M. 2003, ApJ, 593, 630
Maier, C., Meisenheimer, K., Thommes, E., et al. 2003, A&A, 402, 79
Malhotra, S., & Rhoads, J. E. 2002, ApJL, 565, L71
Malhotra, S., & Rhoads, J. E. 2004, ApJL, 617, L5
Martin, C., Sawicki, M., Dressler, A.,& McCarthy, P.J. 2005, NewAR, 50, 53
Neufeld, D. A. 1990, ApJ, 350, 216
Noll, S., Mehlert, D., Appenzeller, I., et al. 2004, A&A, 418, 885
Ouchi, M., Shimasaku, K.,& Okamura, S. 2004, ApJ, 611, 685
Ouchi, M., Shimasaku, K., Akiyama, M., et al. 2005, ApJ, 620, 1
Osterbrock, D. E. 1989, "Astrophysics of Gaseous Nebulae and Active Galactic Nuclei", University Science Books
Rhoads, J. E., Malhotra, S., Dey, A., et al. 2000, ApJ, 545, 85
Rhoads, J. E., Dey, A., Malhotra, S., et al. 2003, AJ, 125, 1006
Rhoads, J. E., Xu, C., Dawson, S., et al. 2004, ApJ, 611, 59
Santos, M. R., Ellis, R. S., Kneib, J.-P., Richard, J.,& Kuijken, K. 2004, ApJ, 606, 683
Shapley, A. E., Steidel, C. C., Pettini, M., & Adelberger, K. L. 2003, ApJ, 588, 65
Snigula, J., Drory, N., Bender R., et al. 2002, MNRAS, 336, 1329
Steidel, C. C., Adelberger, K. L., Shapley, A. E., et al. 2000, ApJ, 532, 170
Tapken, C. 2005, Doctoral Thesis, University Heidelberg
Taniguchi, Y., Shioya, Y., Masaru, A., et al. 2003, JKAS, 36, 22
Taniguchi, Y., Ajiki, M.,& Murayama, T. 2003, ApJ, 585, L97
Taniguchi, Y., Ajiki, M., Nagao, T., et al. 2005, PASJ, 57, 165
Thommes, E., & Meisenheimer, K. 2005, A&A, 430, 877
van Breukelen, C., Jarvis, M. J., & Venemans, B. P. 2005, MNRAS, 359, 895
Venemans, B. P., Röttgering, H. J. A., Overzier, R. A., et al. 2004, A&A, 424, L17
Wang, J. X., Malhotra, & S. Rhoads, J. E. 2005, ApJL, 622, L77

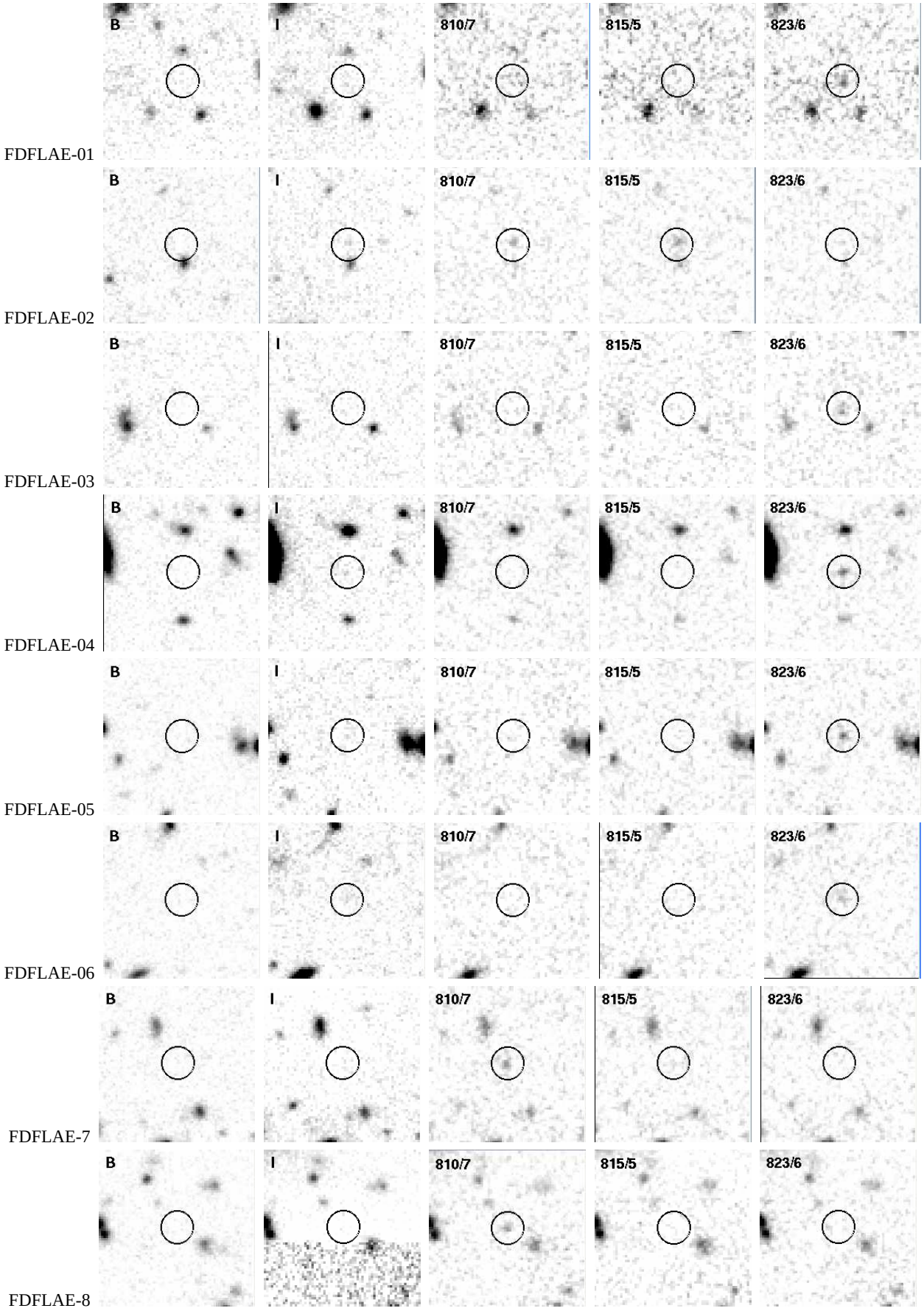

Fig. 9. From left to right: B, I, and narrow-band (810/7, 815/5, 823/6) thumbnail images of Ly-α galaxy candidates FDFLAE-01 to FDFLAE-08 in the FORS Deep Field. The position of the object is marked with a circle. FOV is 20" × 20", North is up, east to the left.

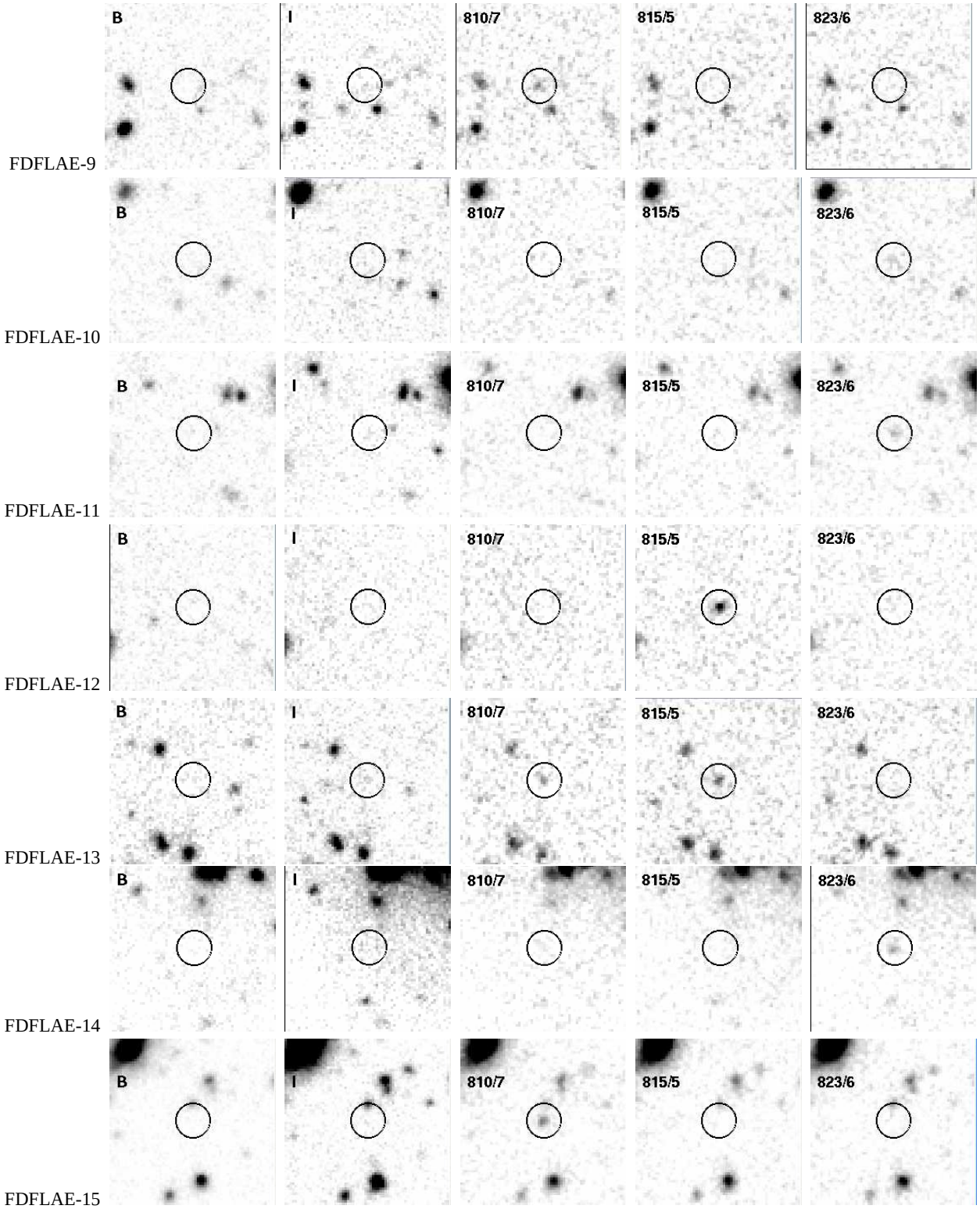

Fig. 9. From left to right: B, I, and narrow-band (810/7, 815/5, 823/6) thumbnail images of Ly-α galaxy candidates FDFLAE-09 to FDFLAE-15 in the FORS Deep Field. The position of the object is marked with a circle. FOV is 20" × 20", North is up, east to the left.